Toepfer *et al. Earth, Planets and Space (2021) 73:204*
https://doi.org/10.1186/s40623-021-01536-8

Earth, Planets and Space

FULL PAPER Open Access

The Mie representation for Mercury's magnetospheric currents

S. Toepfer[1*], Y. Narita[2,3], W. Exner[1,3], D. Heyner[3], P. Kolhey[3], K. -H. Glassmeier[3,4] and U. Motschmann[1,5]

Abstract

Poloidal–toroidal magnetic field decomposition is a useful application of the Mie representation and the decomposition method enables us to determine the current density observationally and unambiguously in the local region of magnetic field measurement. The application and the limits of the decomposition method are tested against the Mercury magnetic field simulation in view of BepiColombo's arrival at Mercury in 2025. The simulated magnetic field data are evaluated along the planned Mercury Planetary Orbiter (MPO) trajectories and the current system that is crossed by the spacecraft is extracted from the magnetic field measurements. Afterwards, the resulting currents are classified in terms of the established current system in the vicinity of Mercury.

Keywords: Poloidal–toroidal decomposition, Magnetospheric current systems, Capon's method

Graphical Abstract

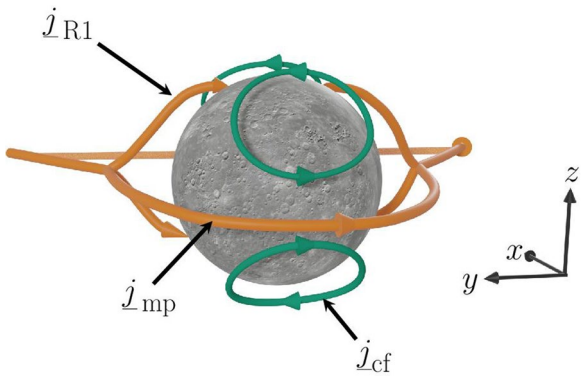

Introduction

The fluxgate magnetometer (Glassmeier et al. 2010; Heyner et al. 2021) on board the Mercury Planetary Orbiter (MPO) of the BepiColombo mission (Benkhoff et al. 2010) will provide precise measurements of the magnetic field in the vicinity of Mercury which enable the detailed characterization of Mercury's internal magnetic field. Due to the plasma physical interaction of Mercury with the solar wind, the measurements are composed of the desired internal contributions as well as external fields resulting from currents flowing within the magnetosphere. For the reconstruction of the internal field, each contribution has to be parametrized properly. Besides the reconstruction of the internal magnetic field, the characterization of the magnetic field contributions within the

*Correspondence: s.toepfer@tu-braunschweig.de
[1] Institut für Theoretische Physik, Technische Universität Braunschweig, Mendelssohnstraße 3, 38106 Braunschweig, Germany
Full list of author information is available at the end of the article

magnetosphere allows the analysis of the external field and the corresponding currents that are crossed by the spacecraft. Since the conventionally used Gauss representation (Gauss 1839; Glassmeier and Tsurutani 2014) is based on the irrotational structure of the magnetic field, the Gauss potential theory does not allow to accurately reconstruct the planetary magnetic field if electric currents are flowing outside the planet and actively generate rotational field structures. Typically, magnetospheric models are used to estimate the magnetic field in current-carrying regions (e.g., Korth et al. 2004, 2015, 2017; Alexeev et al. 2008). These models approximate the magnetic field using a system of modules for the internal field and the fields generated by the tail and the magnetopause currents. As an alternative for the application of global magnetospheric models a combination of the Gauss representation with the Mie representation (toroidal–poloidal decomposition) (Backus 1986, 1996; Olsen 1997), called the Gauss–Mie representation (Toepfer et al. 2021a), enables the parametrization of the magnetic field in current-carrying regions. This parametrization generalizes the international geomagnetic reference field (IGRF) model for the Earth's core field (Thébault et al. 2015) and has successfully been applied in order to reconstruct Mercury's internal magnetic field from simulated magnetic field data (Toepfer et al. 2021a) as well as for the description of the Earth's magnetosphere (Andreeva and Tsyganenko 2016). Especially, the Gauss–Mie representation delivers an analytical parametrization for the magnetic field and therefore enables the analytical calculation of the (local) current density that is crossed by the spacecraft. Within the Earth's magnetosphere the Gauss–Mie representation has successfully been applied to reconstruct ionospheric F-layer currents from MAGSAT and Champ data (Olsen 1997; Engels and Olsen 1999; Bayer 2001; Mayer and Maier 2006). Tsyganenko et al. (2021) reconstructed magnetospheric storm-time dynamics within the terrestrial magnetosphere using the Mie representation. Furthermore, the magnetic field can be parametrized via Euler potentials (e.g., Stern 1967, 1970; Cheng and Zaharia 2003; Romashets and Vandas 2020).

The goal of our study is the determination of the poloidal and toroidal current density flowing in Mercury's magnetosphere in order to validate the parametrization of the magnetic field via the Gauss–Mie representation for the reconstruction of Mercury's internal magnetic field (Toepfer et al. 2021a). In preparation for the observations soon to be obtained by the BepiColombo mission, the plasma interaction of Mercury with the solar wind is simulated numerically using the 3D hybrid model AIKEF (adaptive ion kinetic electron fluid) (Müller et al. 2011). First of all, the established current system at Mercury in comparison with the Earth's magnetosphere is summarized. Then the mathematical foundations of the Gauss–Mie representation are revisited and the parametrization is applied in order to reconstruct poloidal and toroidal currents in Mercury's magnetosphere flowing in the vicinity of the trajectories of the Mercury Planetary Orbiter (MPO) from the simulated magnetic field data. After the reconstruction of the currents, the question arises how these currents are related to a current system around Mercury and how this current system is closed. In analogy to the Earth the structure of Mercury's magnetosphere depends on the orientation of the interplanetary magnetic field (IMF) (e.g., Grygorov et al. (2017)). Thus, the resulting poloidal and toroidal current systems are presented for six different IMF-orientations which may be regarded as mathematical basis orientations.

Current system at Mercury

Before reconstructing the currents in the vicinity of the planned MPO trajectories, we shortly summarize the established current system at Mercury. As the solar wind is a highly conducting medium, Mercury's internal magnetic field is unable to penetrate the solar wind plasma. Therefore, the internal field is compressed at the dayside and stretched into a tail along the nightside. This deformation of the irrotational internal magnetic field is associated with currents flowing in the magnetosphere. In comparison to the Earth's magnetic field, Mercury's internal magnetic field is much weaker so that Mercury's magnetosphere is much smaller than the Earth's magnetosphere. Since the internal dipole moments of both the planets are orientated nearly antiparallel to the planetary rotation axis, the shape of the magnetospheres is comparable. Therefore, the Chapman–Ferraro currents j_{cf} and especially the equatorial magnetopause current j_{mp} isolating the internal magnetic field from the solar wind plasma as well as the neutral sheet current j_{ns} in the tail are qualitatively the same (e.g., Glassmeier (2000)).

Within the Earth's magnetosphere the existence of a dense ionosphere is of major importance for the current closing of field-aligned currents (Iijima and Potemra 1976; Glassmeier 2000). In contrast to the Earth, Mercury does not possess an ionosphere consisting of a dense plasma with a high electrical conductivity, where these currents can be closed. Since the physical and chemical constitution of Mercury's surface is not fully resolved yet, the question whether the field-aligned currents at Mercury are able to penetrate the surface is under debate for decades (e.g., Glassmeier 2000; Janhunen 2004). The analysis of spectrometer data from the MESSENGER mission suggests the existence of an exosphere which is mainly composed of sodium ions Na^+ (Korth et al. 2014; Raines et al. 2014, 2015; James et al. 2019). However, the

absolute value of the sodium ion density, ranging from $5.1 \times 10^{-3}\,\mathrm{cm}^{-3}$ up to $22\,\mathrm{cm}^{-3}$ is still under discussion. Hybrid simulations of the plasma interaction of Mercury with the solar wind considering the existence of a dense sodium exosphere show that Region 1 currents j_{R1} are able to close within the exosphere (Exner et al. 2020). On the other hand, the analysis of MESSENGER magnetic field data indicates the closing of field-aligned currents through Mercury's surface (Anderson et al. 2014).

Since the significance of Mercury's exosphere is still under debate, it is not clear whether Region 2 currents as well as fully developed ring currents occur within Mercury's magnetosphere (e.g., Glassmeier 2000; Baumjohann et al. 2010; Exner et al. 2020). In Table 1, the established current system at Mercury in comparison with the Earth's magnetosphere is summarized.

Although the magnetospheres of Mercury and the Earth are qualitatively comparable, it should be noted that the physical processes for the current closure within the magnetospheres differ from each other (e.g., Glassmeier (2000)). Due to its high electrical conductivity the ability for the closing of magnetospheric currents even without the existence of an ionosphere may be attributed to the plasma. Therefore, it is debatable, whether the naming of the currents that has been established within the description of the Earth's magnetosphere (e.g., Region 1 current) is directly transferable onto the naming of the currents flowing in Mercury's magnetosphere.

Characterization of the magnetic field and the current density

In the following, the basic ideas of the Gauss–Mie representation for modeling the magnetic field and the current density, based on the works of Backus (1986, 1996), Olsen (1997) and Toepfer et al. (2021a) are shortly revisited.

Characterization of the magnetic field

The magnetic field $\underline{B}$ will be measured around Mercury along elliptic orbits like that of the MPO spacecraft. Conceptually covering the orbits by a spherical shell with inner radius a, outer radius c and mean radius $b = (a + c)/2$ enables us to distinguish between different magnetic field contributions. Due to the superposition principle, the total measured field can be written as

$$\underline{B} = \underline{B}^i + \underline{B}^e + \underline{B}^{sh}_T + \underline{B}^{sh}_P, \tag{1}$$

which is called the Gauss–Mie representation of the magnetic field (Toepfer et al. 2021a). The internal field $\underline{B}^i$ results from currents flowing beneath the shell in the region $r < a$. Thus, $\underline{B}^i$ is purely poloidal and especially irrotational within the shell. The currents flowing above the shell ($r > c$) generate an external field structure $\underline{B}^e$ of the same character. Therefore, these contributions can be parametrized via the Gauss representation (Gauss 1839; Glassmeier and Tsurutani 2014) and thus, there exist scalar potentials Φ^i and Φ^e with

$$\underline{B}^i = -\partial_{\underline{x}}\Phi^i, \tag{2}$$

and

$$\underline{B}^e = -\partial_{\underline{x}}\Phi^e. \tag{3}$$

Using body-fixed planetary-centered spherical coordinates with radius $r \in [R_{\mathrm{M}}, \infty)$, azimuth angle $\lambda \in [0, 2\pi]$ and co-latitude $\theta \in [0, \pi]$, the corresponding scalar potentials Φ^i and Φ^e are given by

$$\Phi^i = R_{\mathrm{M}} \sum_{l=1}^{\infty} \sum_{m=0}^{l} \left(\frac{R_{\mathrm{M}}}{r}\right)^{l+1} \left[g_l^m \cos(m\lambda) + h_l^m \sin(m\lambda)\right] P_l^m(\cos(\theta)) \tag{4}$$

and

$$\Phi^e = R_{\mathrm{M}} \sum_{l=1}^{\infty} \sum_{m=0}^{l} \left(\frac{r}{R_{\mathrm{M}}}\right)^{l} \left[q_l^m \cos(m\lambda) + s_l^m \sin(m\lambda)\right] P_l^m(\cos(\theta)), \tag{5}$$

where R_{M} is the planetary radius of Mercury and P_l^m are the Schmidt-normalized associated Legendre polynomials of degree l and order m (Gauss 1839; Glassmeier and Tsurutani 2014). The expansion coefficients g_l^m and h_l^m are the Gauss coefficients for the internal field, the coefficients q_l^m and s_l^m are the Gauss coefficients for the external field, respectively.

Table 1 Established current system at Mercury in comparison with the Earth's magnetosphere

	Earth	Mercury
Dense iono-/exosphere	Yes	Unknown
Magnetopause currents	Yes	Yes
Neutral sheet current	Yes	Yes
Region 1 currents	Yes	Yes
Region 2 currents	Yes	Unknown
Ring current	Yes	Unknown

The currents flowing within the shell in the region $a < r < c$ generate (completely rotational) toroidal $\underline{B}_T^{sh}$ and (potentially rotational) poloidal $\underline{B}_P^{sh}$ magnetic field structures that can be parametrized via the Mie representation (Backus 1986, 1996; Olsen 1997) by making use of scalar functions Ψ_T^{sh} and Ψ_P^{sh}, so that

$$\underline{B}_T^{sh} = \partial_{\underline{x}} \times \left(\Psi_T^{sh} \underline{r} \right) \tag{6}$$

and

$$\underline{B}_P^{sh} = \partial_{\underline{x}} \times \left[\partial_{\underline{x}} \times \left(\Psi_P^{sh} \underline{r} \right) \right] \tag{7}$$

is valid, where $\underline{r} = r\,\underline{e}_r$ and $\underline{e}_r$ is the unit vector in radial direction. The functions Ψ_T^{sh} and Ψ_P^{sh} can be interpreted as a special case of the Euler potentials (Stern 1967, 1970), as shown within the Appendix. Because of the underlying spherical geometry it is straightforward to expand the scalar functions Ψ_T^{sh} and Ψ_P^{sh} into spherical harmonics in analogy to the scalar potentials. Since the exact radial dependence of the corresponding expansion coefficients is unknown, it is useful to perform a Taylor series expansion for the coefficients with respect to the radius r in the vicinity of the mean radius b of the spherical shell (Toepfer et al. 2021a), providing us

$$\Psi_T^{sh} = \frac{R_{\mathrm{M}}}{r} \sum_{l=1}^{\infty} \sum_{m=0}^{l} \left[\alpha_l^m + \alpha_l'^m \, \rho + \mathcal{O}(\rho^2) \right] P_l^m(\cos(\theta)) \tag{8}$$

and

$$\Psi_P^{sh} = \frac{R_{\mathrm{M}}^2}{r} \sum_{l=1}^{\infty} \sum_{m=0}^{l} \left[\beta_l^m + \beta_l'^m \, \rho + \mathcal{O}(\rho^2) \right] P_l^m(\cos(\theta)), \tag{9}$$

where

$$\begin{aligned} \rho &= (r - b)/R_{\mathrm{M}}, \\ \alpha_l^m &= a_l^m \cos(m\lambda) + b_l^m \sin(m\lambda), \\ \alpha_l'^m &= a_l'^m \cos(m\lambda) + b_l'^m \sin(m\lambda), \\ \beta_l^m &= c_l^m \cos(m\lambda) + d_l^m \sin(m\lambda), \\ \beta_l'^m &= c_l'^m \cos(m\lambda) + d_l'^m \sin(m\lambda). \end{aligned}$$

Theoretically, the functions Ψ_P^{sh} and Ψ_T^{sh} as well as the potentials Φ^i and Φ^e have to be expanded into a series containing an infinite set of basis functions. Within the practical application, the summations have to be truncated at a suitable degree $l < \infty$, where it is desirable to incorporate as less terms as possible. On the other hand, the magnetic field has to be parametrized adequately. Thus, it is useful to choose a manageable ansatz for the series expansion which can be extended gradually.

Inserting the parametrization of the magnetic field contributions into Eq. (1) delivers

$$\underline{B} = -\partial_{\underline{x}} \Phi^i - \partial_{\underline{x}} \Phi^e + \partial_{\underline{x}} \times \left(\Psi_T^{sh} \underline{r} \right) + \partial_{\underline{x}} \times \left[\partial_{\underline{x}} \times \left(\Psi_P^{sh} \underline{r} \right) \right]. \tag{10}$$

Rearranging the terms of the series expansions into the shape matrices $\underline{\underline{H}}^i$, $\underline{\underline{H}}^e$, $\underline{\underline{H}}_T^{sh}$ and $\underline{\underline{H}}_P^{sh}$ and summarizing the corresponding expansion coefficients into the vectors $\underline{g}^i$, $\underline{g}^e$, $\underline{g}_T^{sh}$ and $\underline{g}_P^{sh}$, the Gauss–Mie representation of the magnetic field can be rewritten in the linear algebraic form

$$\underline{B} = \underline{\underline{H}}^i \underline{g}^i + \underline{\underline{H}}^e \underline{g}^e + \underline{\underline{H}}_T^{sh} \underline{g}_T^{sh} + \underline{\underline{H}}_P^{sh} \underline{g}_P^{sh}. \tag{11}$$

The $\underline{\underline{H}}$s mainly contain well-known information about the positions, whereas the $\underline{g}$s are the unknown coefficients which need to be determined from the measurements.

For the reconstruction of Mercury's internal magnetic field, the application of the thin shell approximation (Backus 1986, 1996; Olsen 1997; Toepfer et al. 2021a) is a valid assumption. The thin shell approximation allows the negligence of the poloidal field $\underline{B}_P^{sh}$ generated by toroidal currents flowing within the shell, when the width of the shell is smaller than the length scale on which the currents change in radial direction. For the analysis of the full current density inside the shell this negligence, in turn, causes a problem, as for this purpose the knowledge of $\underline{B}_P^{sh}$ is indispensable. The way out works as follows. After the application of the thin shell approximation, the internal Gauss coefficients g_l^m and h_l^m, the external Gauss coefficients q_l^m and s_l^m as well as the expansion coefficients a_l^m, b_l^m, $a_l'^m$, $b_l'^m$ for the toroidal magnetic field can be estimated by making use of a suitable inversion method such as Capon's method (Capon 1969; Motschmann et al. 1996; Toepfer et al. 2020b, 2021b), that serves as a powerful tool for the analysis of planetary magnetic fields (Toepfer et al. 2020a). Afterwards, the expansion coefficients c_l^m, d_l^m, $c_l'^m$, $d_l'^m$ for the poloidal magnetic field can be estimated by obtaining an approximate solution of

$$\underline{B}_P^{sh} = \underline{B} - \left(\underline{B}^i + \underline{B}^e + \underline{B}_T^{sh} \right) = \underline{\underline{H}}_P^{sh} \underline{g}_P^{sh} \tag{12}$$

for the coefficient vector $\underline{g}_P^{sh}$. It should be noted that the expansion coefficients for the poloidal magnetic field cannot be estimated simultaneously with the internal

and external Gauss coefficients. As discussed in Toepfer et al. (2021a), these fields follow the same topological structure, so that the poloidal field $\underline{B}_P^{sh}$ cannot be distinguished from the internal $\underline{B}^i$ and external field $\underline{B}^e$ within the reconstruction procedure.

Characterization of the current density

After the reconstruction of the poloidal $\underline{g}_P^{sh}$ and toroidal coefficients $\underline{g}_T^{sh}$ from the magnetic field data, the corresponding current density $\underline{j}^{sh}$ flowing within the shell can be determined using Ampère's law

$$\underline{j}^{sh} = \frac{1}{\mu_0}\partial_{\underline{x}} \times \underline{B}, \tag{13}$$

so that $\underline{j}^{sh}$ describes a solenoidal vector field. Inserting the parametrization of the magnetic field (cf. Equation 1) and using

$$\partial_{\underline{x}} \times \underline{B}^i = 0 = \partial_{\underline{x}} \times \underline{B}^e, \tag{14}$$

the current density within the shell is given by

$$\underline{j}^{sh} = \frac{1}{\mu_0}\partial_{\underline{x}} \times \underline{B} = \frac{1}{\mu_0}\partial_{\underline{x}} \times \underline{B}_T^{sh} + \frac{1}{\mu_0}\partial_{\underline{x}} \times \underline{B}_P^{sh}. \tag{15}$$

Considering the divergence-free nature of the current density (no charge accumulation), $\underline{j}^{sh}$ can be decomposed into its toroidal part

$$\begin{aligned}\underline{j}_T^{sh} &= \frac{1}{\mu_0}\partial_{\underline{x}} \times \underline{B}_P^{sh} = \frac{1}{\mu_0}\partial_{\underline{x}} \times \partial_{\underline{x}} \times \left[\partial_{\underline{x}} \times \left(\Psi_P^{sh}\underline{r}\right)\right] \\ &= \frac{1}{\mu_0}\partial_{\underline{x}} \times \left[\left(-\partial_{\underline{x}}^2\Psi_P^{sh}\right)\underline{r}\right]\end{aligned} \tag{16}$$

and poloidal part

$$\underline{j}_P^{sh} = \frac{1}{\mu_0}\partial_{\underline{x}} \times \underline{B}_T^{sh} = \frac{1}{\mu_0}\partial_{\underline{x}} \times \left[\partial_{\underline{x}} \times \left(\Psi_T^{sh}\underline{r}\right)\right] \tag{17}$$

in analogy to the magnetic field. Thus,

$$\partial_{\underline{x}} \cdot \underline{j}_P^{sh} = 0 \tag{18}$$

and simultaneously

$$\partial_{\underline{x}} \cdot \underline{j}_T^{sh} = 0 \tag{19}$$

hold so that the poloidal and the toroidal current systems are closed independently of each other.

Application to simulated Mercury magnetic field data

For a first validation of the Gauss–Mie representation suggested here to reconstruct the current density $\underline{j}^{sh}$ in the vicinity of the planned MPO orbits, simulated stationary magnetic field data and electric currents system information based on using the AIKEF hybrid code (electron fluid, kinetic ions) (Müller et al. 2011) are analyzed. This code has successfully been applied to several problems in Mercury's plasma interaction (e.g., Exner et al. 2018, 2020). From the simulated magnetic field data, the current system is derived using the above described new approach and the results are compared with the electric currents directly derived from the simulation.

Mercury's internal magnetic field is modeled as a dipole field with an internal dipole moment of −190 nT, which is shifted northward by $0.2\,R_{\mathrm{M}}$. This field can equivalently be described as a multipole field with the internal Gauss coefficients $g_1^0 = -190\,\mathrm{nT}$ for the dipole field, $g_2^0 = -78\,\mathrm{nT}$ for the quadrupole field and $g_3^0 = -20\,\mathrm{nT}$ for the octupole field (Anderson et al. 2012; Wardinski et al. 2019). The internal Gauss coefficients determining the internal stationary magnetic field are implemented in the simulation code and the plasma interaction of Mercury with the solar wind is simulated. The interplanetary magnetic field with a magnitude of $B_{\mathrm{IMF}} = 20\,\mathrm{nT}$ (Winslow et al. 2013) is orientated along the vector $(x,y,z)^T = (0,0,-1)^T$ in the Mercury-Anti-Solar-Orbital coordinate system (MASO), i.e., the x-axis is orientated towards the nightside of Mercury (away from the sun), the z-axis is orientated parallel to the rotation axis (i.e., antiparallel to the internal dipole moment) and the y-axis completes the right hand system. The solar wind velocity of $u_{\mathrm{sw}} = 400\,\mathrm{km/s}$ points along the x-axis and the solar wind proton density was chosen to $n_{\mathrm{sw}} = 30\,\mathrm{cm}^{-3}$ (cf. Winslow et al. (2013)). Mercury's outer mantle ($0.7\,R_{\mathrm{M}} \le r \le 1\,R_{\mathrm{M}}$) is modeled with a radially symmetric planetary resistivity profile with a resistivity of $\eta_S \approx 840\,\mathrm{k}\Omega m$ (or conductivity of $10^{-6}\,\mathrm{S/m}$) at the surface and the core possesses a vanishing resistivity (Jia et al. 2015; Exner et al. 2018, 2020). The influence of Mercury's exosphere is neglected, since the plasma interaction is only affected by the exosphere in the case of an extremely high ion density and the absolute value of the density is unknown (Exner et al. 2020). The resulting simulated magnetic field data are evaluated along the ellipsoid

$$\mathcal{E} = \left\{(x,y,z)^T \,\middle|\, \frac{(x-0.2\,R_{\mathrm{M}})^2}{(1.4\,R_{\mathrm{M}})^2} + \frac{y^2}{(1.2\,R_{\mathrm{M}})^2} + \frac{z^2}{(1.16\,R_{\mathrm{M}})^2} = 1\right\}, \tag{20}$$

which describes the envelope of the elliptical MPO orbit rotated in longitudinal direction from −50° (afternoon/post-midnight sector) over 0° (noon/midnight, x–z-plane) to 50° (morning/pre-midnight sector) around the rotation axis (z-axis).

For the reconstruction of the current density $\underline{j}^{sh}$ from the magnetic field data $\underline{B}$, the scalar potentials Φ^i, Φ^e of the internal and external fields are expanded into spherical harmonics up to the third degree and order representing the internal/external dipole, quadrupole and octupole field. The scalar functions Ψ_P^{sh}, Ψ_T^{sh} of the poloidal and toroidal magnetic fields are expanded into spherical harmonics up to the fourth degree and order. Furthermore, the scalar function Ψ_P^{sh} is expanded into a Taylor series with respect to the radius r in the vicinity of the mean radius b of the spherical shell up to the first order. The function Ψ_T^{sh} is cut off at the zeroth order for the radius describing the influence of the radial currents (Toepfer et al. 2021a) since it is expectable that the radial currents are the dominating poloidal currents in the vicinity of the surface. Thus, the magnetic field is modeled with 102 expansion coefficients in the data analysis, i.e., 15 internal Gauss coefficients, 15 external Gauss coefficients, 24 toroidal coefficients, 48 poloidal coefficients. As a proof of concept, the maximum orders of the series expansions are chosen to achieve a reasonable qualitative agreement between the simulated and the reconstructed currents. For a detailed quantitative analysis, it is worthwhile to incorporate higher orders of the series expansions. The wanted expansion coefficients are estimated with Capon's method (Capon 1969; Motschmann et al. 1996; Toepfer et al. 2020a, b, 2021b) from the simulated magnetic field data. Afterwards, the estimated expansion coefficients $\underline{g}_P^{sh}$ for the poloidal magnetic field and the coefficients $\underline{g}_T^{sh}$ for the toroidal magnetic field are used to reconstruct the current density $\underline{j}^{sh}$ (cf. Equation 15) within the shell.

The simulated and the reconstructed current density $\underline{j}^{sh}$ along the ellipsoid $\mathcal{E}$ on the nightside and dayside of Mercury are displayed in Figs. 1 and 2, respectively. The simulated current system is dominated by equatorial currents flowing from dawn ($y > 0$) to dusk ($y < 0$) at the nightside (red arrows in Fig. 1a) and vice versa at the dayside (red arrows in Fig. 2a). The reconstructed equatorial currents (yellow arrows in Fig. 1b and green arrows in Fig. 2b) follow this geometry. At the nightside, the equatorial currents split into a current flowing towards Mercury at the dawnside and depart from the planet at the duskside. The polar regions are characterized by horizontal currents. At the northern pole, the currents penetrate the surface in the region $y > 0$ (green arrows in Fig. 2a, yellow arrows in Fig. 2b) and leave the planet at $y < 0$ (red arrows in Fig. 2a, red arrows in Fig. 2b). It should be noted that the reconstructed currents are calculated analytically and therefore, the reconstruction is smoother than the numerical simulation. However, the reconstruction method reproduces the structure of the simulated currents (cf. Figs. 1b and 2b) and thus, the Mie representation is capable of describing the geometrical nature of the currents flowing in the vicinity of the MPO orbit.

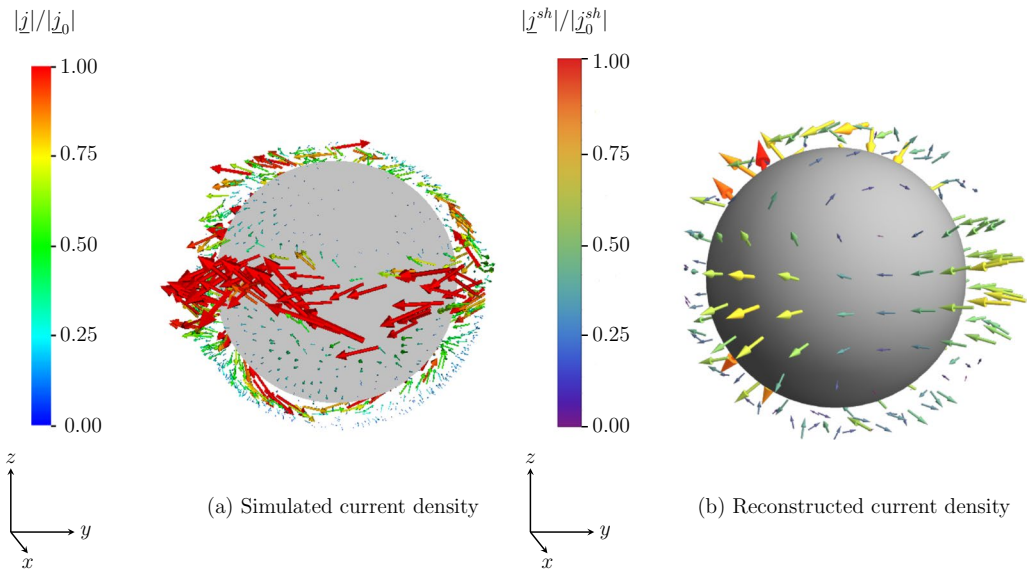

Fig. 1 Simulated current density in multiples of $|\underline{j}_0| = 40\,\mathrm{nA/m^2}$ and reconstructed current density in multiples of $|\underline{j}_0^{sh}| = 25\,\mathrm{nA/m^2}$ along the ellipsoid $\mathcal{E}$ on the nightside of Mercury

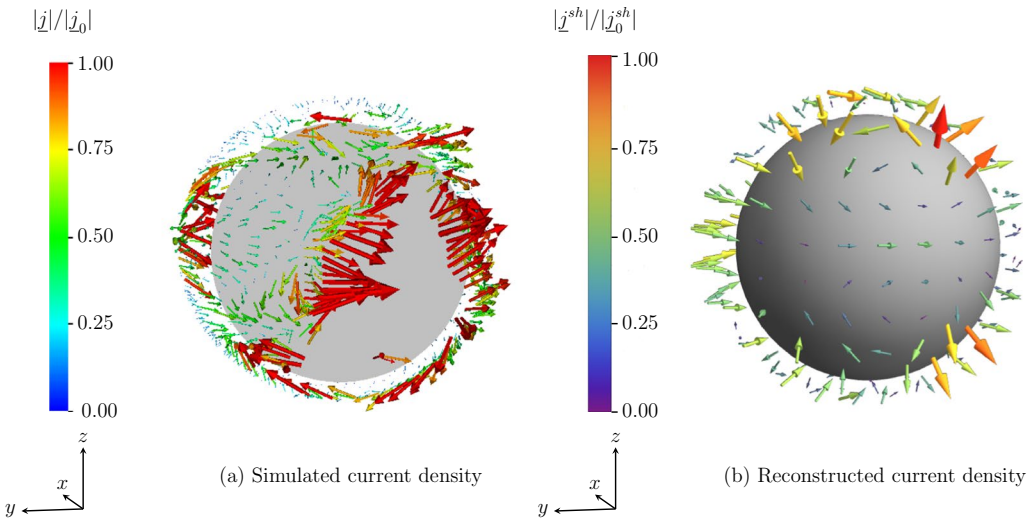

Fig. 2 Simulated current density in multiples of $|\underline{j}_0| = 40\,\mathrm{nA/m^2}$ and reconstructed current density in multiples of $|\underline{j}_0^{sh}| = 25\,\mathrm{nA/m^2}$ along the ellipsoid $\mathcal{E}$ on the dayside of Mercury

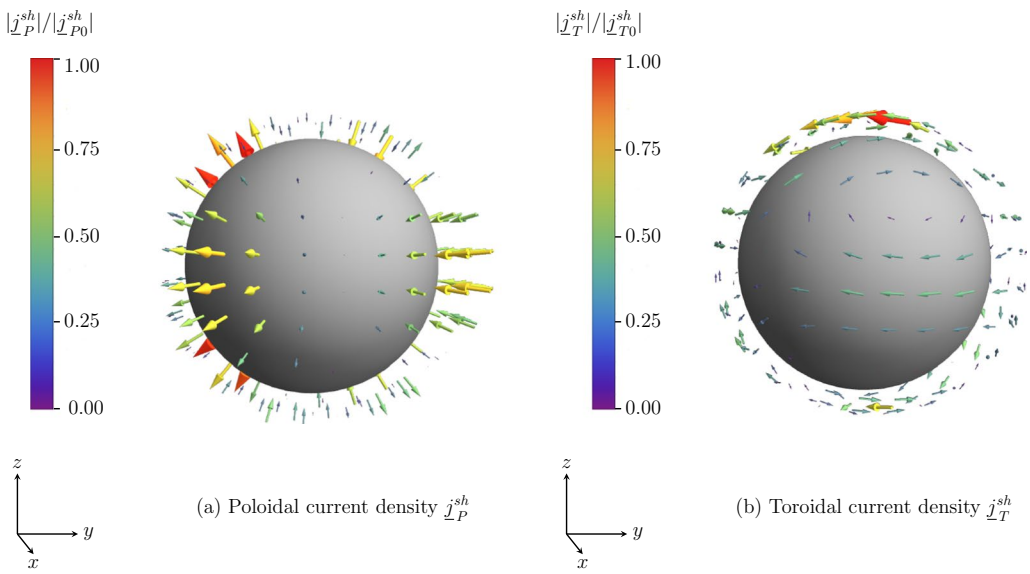

Fig. 3 Decomposition of the reconstructed current density j^{sh} into its poloidal and toroidal parts along the ellipsoid $\mathcal{E}$ on the nightside of Mercury. The poloidal current density is presented in multiples of $|\underline{j}_{P0}^{sh}| = 25\,\mathrm{nA/m^2}$ and the toroidal current density is given in multiples of $|\underline{j}_{T0}^{sh}| = 15\,\mathrm{nA/m^2}$

Furthermore, the simulated and the reconstructed current densities are of the same order. The magnitude of the reconstructed current density with a maximum amplitude of about $20\,\mathrm{nA/m^2}$ up to $25\,\mathrm{nA/m^2}$ in the polar regions differs only by the factor two from the simulated magnitude with a maximum value of about $40\,\mathrm{nA/m^2}$ in the polar regions. Since the scalar functions Ψ_P^{sh} and Ψ_T^{sh} are expanded into spherical harmonics up to the fourth degree and order, it is expectable that the extension of the series expansion by degrees $l > 4$ will close the void between the reconstructed and the simulated magnitude of the current density.

Figure 3 displays the poloidal $\underline{j}_P^{sh}$ and toroidal parts $\underline{j}_T^{sh}$ of the reconstructed current density. The toroidal currents are characterized by closed loops with the divergence-free nature of $\underline{j}_T^{sh}$ being immediately visible. Since the radial (poloidal) currents cross the ellipsoid $\mathcal{E}$, from the first point of view it is not obvious how these currents are closed. Moreover, the magnitude of the toroidal current density with a maximum value of $\left|\underline{j}_T^{sh}\right| \approx 15\,\mathrm{nA/m^2}$ at the northern pole is smaller than the magnitude of the poloidal current density ($\left|\underline{j}_P^{sh}\right| \approx 20\,\mathrm{nA/m^2}$ up to $25\,\mathrm{nA/m^2}$ at the northern pole), but both the magnitudes are of the same order.

Poloidal and toroidal current systems under different IMF-orientations

The simulated current density has reasonably been reconstructed from the simulated magnetic field data. Now, the question arises how the currents are related to the current system around Mercury presented in the section "Current system at Mercury" and how the poloidal currents are closed.

Besides the geometry of the internal magnetic field the current system depends on the direction of the interplanetary magnetic field (IMF) (Ganushkina et al. 2015; Milan et al. 2017; Ganushkina et al. 2018). To investigate the qualitative structure of the current system around Mercury, simulated stationary magnetic field data and current densities resulting from the plasma interaction of Mercury with the solar wind under different IMF-orientations, i.e., $\underline{B}_{\mathrm{IMF}} = \pm 20\,\mathrm{nT}\,\underline{e}_x$, $\underline{B}_{\mathrm{IMF}} = \pm 20\,\mathrm{nT}\,\underline{e}_y$, $\underline{B}_{\mathrm{IMF}} = \pm 20\,\mathrm{nT}\,\underline{e}_z$, where $\underline{e}_x$, $\underline{e}_y$ and $\underline{e}_z$ are the unit vectors of the corresponding main axes in the MASO system, are analyzed. Although Mercury's magnetosphere is a highly dynamic system, the interplanetary magnetic field in the vicinity of Mercury's orbit can be regarded as stationary for a time period of 20–40 min in times of a calm upstream solar wind (He et al. 2017; James et al. 2017). The resulting poloidal and toroidal current systems on the nightside and on the dayside of Mercury for each IMF-direction are sketched in Figs. 4 and 5.

The dayside current system is dominated by the Chapman–Ferraro currents $\underline{j}_{\mathrm{cf}}$. These currents decompose into poloidal (orange) and toroidal currents (green). The toroidal part of the Chapman–Ferraro currents is characterized by closed loops so that this part of the current system is closed within the magnetospheric plasma. The nightside current system is dominated by the neutral sheet current $\underline{j}_{\mathrm{ns}}$, simplified by just a single dawn–dusk-directed arrow. The magnetopause current $\underline{j}_{\mathrm{mp}}$ as well as the neutral sheet current are connected via poloidal currents at the dawn ($y > 0$) and duskside ($y < 0$) so that both the currents are characterized by a poloidal topology. Since the structure of the magnetopause current and the neutral sheet current is determined by the internal magnetic field, these currents remain qualitatively unchanged for all IMF-directions. In the polar regions the poloidal part of the Chapman–Ferraro currents transits into poloidal Region 1 currents $\underline{j}_{\mathrm{R1}}$. Due to the high conductivity within Mercury's core, the Region 1 currents flowing in radial direction towards the planet at the dawnside and depart from the planet at the duskside are able to penetrate the surface and partially close via the core–mantle boundary, as proposed by Anderson et al. (2014). The currents flowing depart from the planet are closed within the nightside magnetosphere. Within the simulation presented here, no exosphere has been adopted. Considering the influence of Mercury's exosphere on the current system, a significant portion of the Region 1 currents can be closed within a sodium exosphere of sufficient density, in similarity to Earth's ionosphere, as shown by Exner et al. (2020).

Analogously to the plasma interaction of the Earth's magnetic field with the solar wind, there occur field-aligned currents $\underline{j}_{\mathrm{fac}}$ at the northern and at the southern pole in the case of a non-vanishing B_y-component of the IMF (cf. Figs. 4b and 5b) (Leontyev and Lyatsky 1974; Trondsen et al. 1999; Liou and Mitchell 2019). Due to the frozen-in theorem the motional electric field is given by

$$\underline{E}_{\mathrm{IMF}} = -\underline{u}_{\mathrm{sw}} \times \underline{B}_{\mathrm{IMF}}. \tag{21}$$

In the case of $B_y \neq 0$ ($B_x = B_z = 0$), the electric field is orientated (anti-)parallel to the z-axis, since the solar wind velocity is orientated along the x-axis. We find that the field-aligned currents flow towards the planet at the northern pole and depart from the planet at the southern pole in the case of $B_y > 0$ and vice versa in the case of $B_y < 0$.

Furthermore, the IMF-direction determines the symmetry of the magnetosphere. A non-vanishing B_y-component results in dawn–dusk asymmetries within the tail, whereas the B_x-component influences the north–south symmetry of the magnetosphere.

In the case of $B_{\mathrm{IMF}} = 20\,\mathrm{nT}\,\underline{e}_x$ as well as $B_{\mathrm{IMF}} = \pm 20\,\mathrm{nT}\,\underline{e}_y$ (cf. Figs. 4a and b, 5b), within the reconstruction procedure there occur toroidal currents with an amplitude of about $10\,\mathrm{nA/m^2}$ that are oppositely directed to the (poloidal) magnetopause current at the dayside of Mercury and oppositely directed to the (poloidal) neutral sheet current at the nightside. This behavior is founded on the mathematical decomposition of the current density as a vector field. First of all, the quantities $\underline{j}_P^{sh}$ and $\underline{j}_T^{sh}$ are mathematical vector fields, which do not mandatorily exist as physical quantities. Thus, a vanishing current at a point $\underline{x}_0$ can equivalently be described as a superposition of oppositely directed non-vanishing

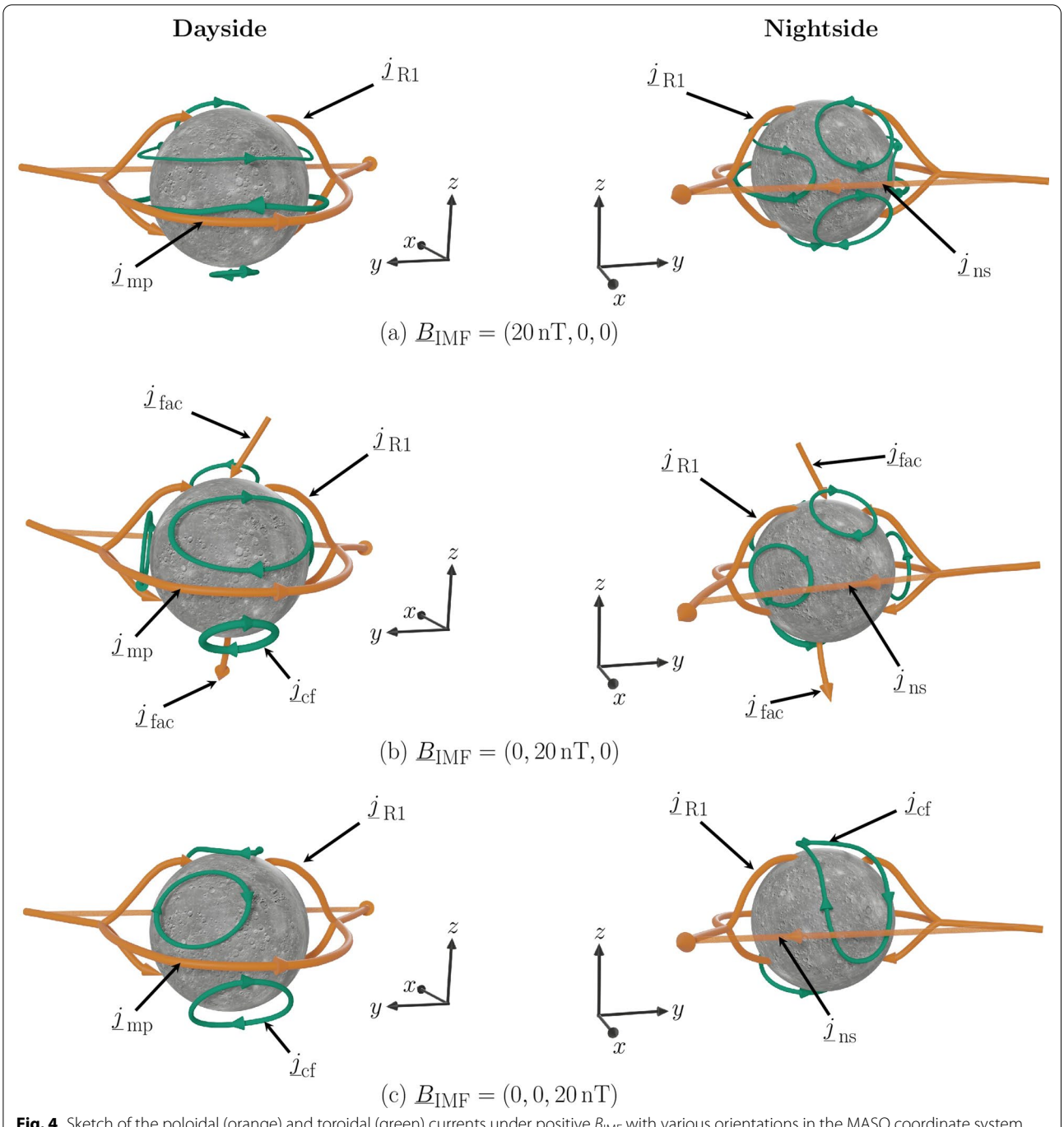

Fig. 4 Sketch of the poloidal (orange) and toroidal (green) currents under positive $\underline{B}_{\mathrm{IMF}}$ with various orientations in the MASO coordinate system

poloidal and toroidal currents with the same magnitude so that

$$\underline{j}_P^{sh}(\underline{x}_0) + \underline{j}_T^{sh}(\underline{x}_0) = 0 \tag{22}$$

is valid locally as schematically sketched in Fig. 6a and b. Due to the finite spatial extent of the currents, at least partially they can flow independently of each other in regions this side of $\underline{x}_0$ or beyond $\underline{x}_0$ (cf. Fig. 6c). Although the total (physical) current $\underline{j}$ is determined by the superposition of the poloidal and the toroidal current, the mathematical decomposition of the current density enables us to predict the potential origin of the current and to analyze the potential trajectories of the

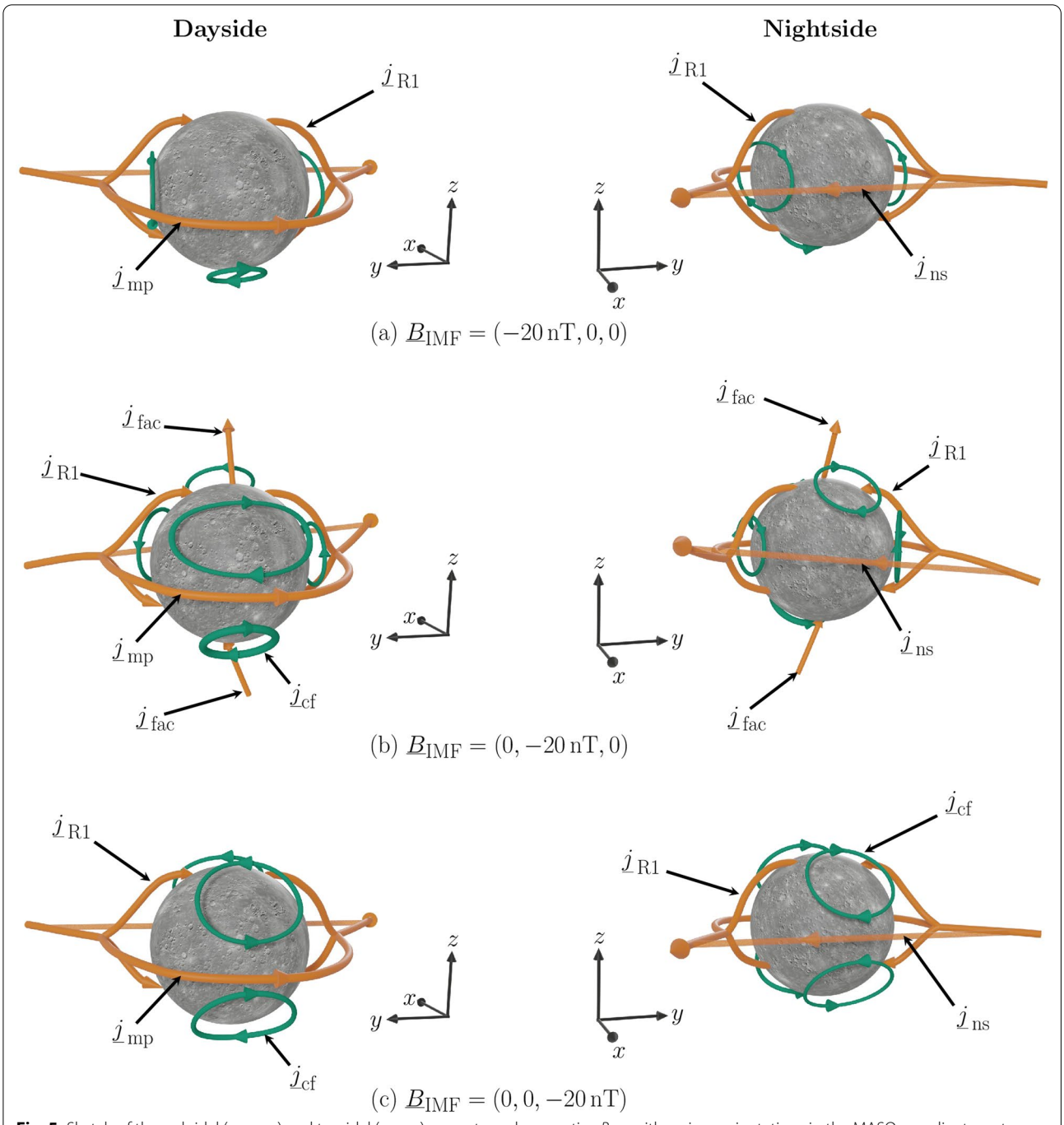

Fig. 5 Sketch of the poloidal (orange) and toroidal (green) currents under negative $\underline{B}_{IMF}$ with various orientations in the MASO coordinate system

particles carrying the current. Thus, the toroidal current flowing antiparallel to the magnetopause current as well as antiparallel to the neutral sheet current can be interpreted as a ring current which superposes with the poloidal neutral sheet current and the magnetopause current. This ring current should be partially trackable along the planned MPO orbits.

In terms of the poloidal–toroidal decomposition, the current system around Mercury as sketched in Figs. 4 and 5 can be summarized as follows. The poloidal current (orange) flows towards Mercury at the dawnside ($y > 0$) and splits into the neutral sheet current $\underline{j}_{ns}$, the

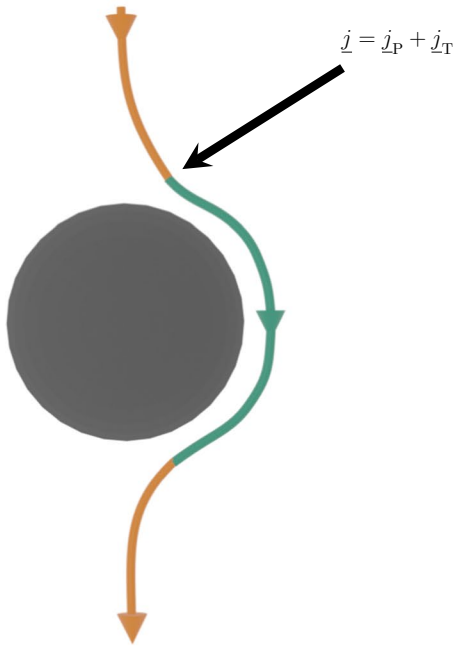

(a) Total current density $\underline{j}$.

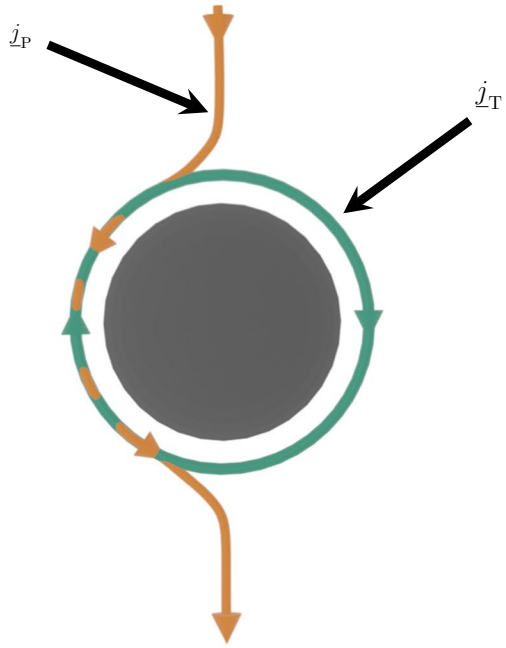

(b) Equivalent decomposition.

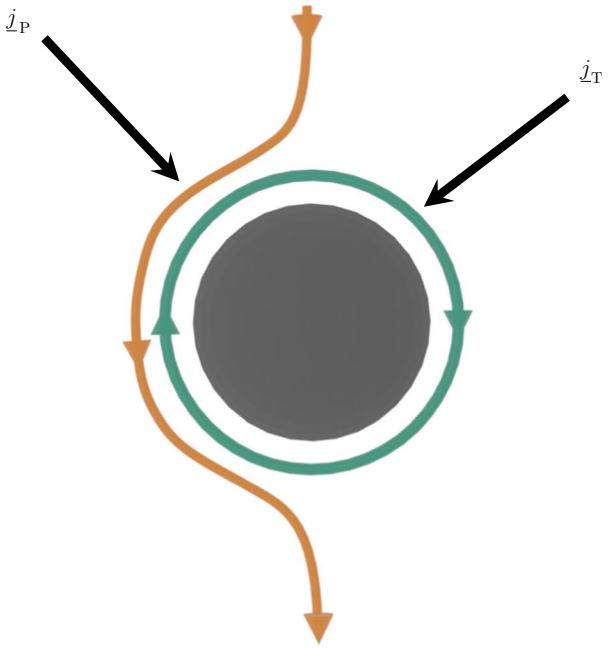

(c) Independent currents.

Fig. 6 Superposition of poloidal (orange) and toroidal (green) currents. A vanishing current density $\underline{j} = 0$ on the left side of the grey sphere (**a**) can equivalently be described as a superposition of non-vanishing poloidal and toroidal currents, so that $\underline{j}_P + \underline{j}_T = 0$ is valid locally (**b**). The currents can flow independently of each other in a certain spatial distance (**c**)

Region 1 current $\underline{j}_{\mathrm{R1}}$ and the dayside magnetopause current $\underline{j}_{\mathrm{mp}}$. The Region 1 currents are able to penetrate the surface. These currents close via the core–mantle boundary and leave the planet at the duskside ($y < 0$), where they reconnect with the magnetopause current and the neutral sheet current. This poloidal current system remains qualitatively similar for all IMF-directions. The toroidal Chapman–Ferraro currents $\underline{j}_{\mathrm{cf}}$ are characterized by closed loops (green). The position of these loops varies for different IMF-orientations. In the case of $B_{\mathrm{IMF}} = 20\,\mathrm{nT}\,\underline{e}_x$ as well as $B_{\mathrm{IMF}} = \pm 20\,\mathrm{nT}\,\underline{e}_y$ the equatorial parts of the loops at the dayside are orientated antiparallel to the magnetopause current as well as antiparallel to the neutral sheet current at the nightside. For a non-vanishing B_y-component, the (poloidal) field-aligned currents $\underline{j}_{\mathrm{fac}}$ at the northern and at the southern pole also penetrate the surface and close via the core–mantle boundary.

Although the plasma interaction of Mercury with the solar wind does not linearily depend on the IMF-orientation, it is expectable that the resulting current system for any other IMF-orientation can be constructed by superposing the cases presented above.

Summary and outlook

The analysis of current systems is of major importance for the comprehension of Mercury's magnetosphere. Since the Mie representation delivers an analytical parametrization for rotational magnetic fields, it enables the analytical calculation of the current density flowing in regions that are crossed by the Mercury Planetary Orbiter (MPO) from the measured magnetic field data. As a proxy for the not yet available MPO data, the magnetic field in the vicinity of Mercury is simulated with the hybrid code AIKEF and the data are evaluated along the planned trajectories of the MPO. The comparison of the simulated and the reconstructed current density shows, that the reconstructed currents are in reasonable agreement with the simulated currents. Thus, the Mie representation serves as a useful model for the analysis of currents that are crossed by the spacecraft. Furthermore, the Mie representation enables the decomposition of the current density into its poloidal and toroidal parts. The reconstructed toroidal currents are characterized by closed loops, whereas the poloidal currents cross the envelope of the trajectories in radial direction. Especially, the mathematical decomposition of the current density enables us to predict the potential origin of the current and to analyze the potential physical trajectories of the particles carrying the current.

After the reconstruction procedure, the question arises how the poloidal currents are closed and how the reconstructed currents are related to a complete current system around Mercury. Since the structure of Mercury's magnetosphere depends on the orientation of the interplanetary magnetic field (IMF), the plasma interaction of Mercury with the solar wind is simulated for six different IMF-directions along the main axes in the MASO system. It turns out that the poloidal current system remains qualitatively unchanged since, for example, the magnetopause current as well as the neutral sheet current is mainly determined by Mercury's internal magnetic field. In the case of a non-vanishing B_y-component of the IMF, there occur field-aligned currents in the polar regions which follow the motional electric field. Furthermore, the non-vanishing B_y-component yields dawn–dusk asymmetries, whereas the existence of a non-vanishing B_x-component violates the north–south symmetry.

Within the present study, the magnetic field data have been evaluated along a complete ellipsoid to reconstruct the current density for each IMF-orientation. Analyzing in situ magnetic field data, the current density can be reconstructed along segments of the MPO orbit for each IMF-orientation and the results can be classified in terms of the complete current system presented here. In addition, it should be noted that the Mie representation requires the series expansion of the magnetic field. Within the practical application, the series expansions have to be truncated at a suitable degree, where the choice of the maximum degree depends on the distribution and the amount of the available data points.

Furthermore, Mercury's exosphere has been neglected within the simulations so that the field-aligned currents close via the core–mantle boundary. Therefore, the influence of Mercury's exosphere on the poloidal and toroidal current systems should be analyzed in future studies. Moreover, it is worthwhile to investigate the influence of dynamical effects on the current system within Mercury's magnetosphere (Korth et al. 2017; Slavin et al. 2021).

Concerning the BepiColombo mission, this work establishes the basis for the application of the Mie representation to calculate currents from the magnetic field measurements analytically and to analyze their poloidal and toroidal contributions.

Appendix

Within the Mie representation the magnetic field can be written as

$$\underline{B} = \partial_{\underline{x}} \times (\Psi_T\, \underline{r}) + \partial_{\underline{x}} \times \left[\partial_{\underline{x}} \times (\Psi_P\, \underline{r})\right] \tag{23}$$

and the corresponding vector potential is given by

$$\underline{A} = \Psi_T \, \underline{r} + \partial_{\underline{x}} \times (\Psi_P \, \underline{r}) \tag{24}$$

$$= \Psi_T r \, \underline{e}_r + \frac{1}{r \sin(\theta)} \partial_\lambda (\Psi_P r) \underline{e}_\theta - \frac{1}{r} \partial_\theta (\Psi_P r) \underline{e}_\lambda, \tag{25}$$

so that $\underline{B} = \partial_{\underline{x}} \times \underline{A}$ is valid (Toepfer et al. 2021a). Alternatively, the magnetic field can be parametrized via Euler potentials α and β (Stern 1967, 1970) resulting in

$$\underline{B} = \partial_{\underline{x}} \alpha \times \partial_{\underline{x}} \beta. \tag{26}$$

The corresponding vector potential can be written as

$$\underline{A} = \alpha \, \partial_{\underline{x}} \beta. \tag{27}$$

The Mie representation is based on the decomposition of the magnetic field with respect to spherical coordinates. Expanding Eq. (27) in spherical coordinates

$$\alpha \, \partial_{\underline{x}} \beta = \alpha \left[\partial_r \beta \, \underline{e}_r + \frac{1}{r} \partial_\theta \beta \, \underline{e}_\theta + \frac{1}{r \sin(\theta)} \partial_\lambda \beta \, \underline{e}_\lambda \right] \tag{28}$$

and comparing the coefficients with Eq. (25) delivers

$$\Psi_T = \frac{\alpha}{r} \partial_r \beta \tag{29}$$

as well as

$$\alpha \, \partial_\theta \beta = \frac{r}{\sin(\theta)} \partial_\lambda \Psi_P, \tag{30}$$

$$\frac{\alpha}{\sin(\theta)} \partial_\lambda \beta = -r \, \partial_\theta \Psi_P. \tag{31}$$

Thus, the scalar functions Ψ_P and Ψ_T can be interpreted as a special case of the Euler potentials α and β.

Acknowledgements
The authors are grateful for stimulating discussions and helpful suggestions by Alexander Schwenke. ST, UM and WE acknowledge the North-German Supercomputing Alliance (HLRN) for providing HPC resources that have contributed to the research results reported in this paper.

Authors' contributions
All authors contributed conception and design of the study; ST and UM wrote the first draft of the manuscript; WE organized the data base; all authors contributed to manuscript revision. All authors read and approved the final manuscript.

Funding
Open Access funding enabled and organized by Projekt DEAL. We acknowledge support by the German Research Foundation and the Open Access Publication Funds of the Technische Universität Braunschweig. The work by Y. Narita is supported by the Austrian Space Applications Programme at the Austrian Research Promotion Agency under contract 865967. D. Heyner and K.-H. Glassmeier were supported by the German Ministerium für Wirtschaft und Energie and the German Zentrum für Luft- und Raumfahrt under contract 50 QW1501. W.E. and D.H. were supported by DFG (German Research Foundation) under contract HE8016/1-1.

Availability of data and materials
Simulation data can be provided upon request.

Declarations

Competing interests
The authors declare that they have no conflict of interest.

Author details
[1]Institut für Theoretische Physik, Technische Universität Braunschweig, Mendelssohnstraße 3, 38106 Braunschweig, Germany. [2]Space Research Institute, Austrian Academy of Sciences, Schmiedlstraße 6, 8042 Graz, Austria. [3]Institut für Geophysik und extraterrestrische Physik, Technische Universität Braunschweig, Mendelssohnstraße 3, 38106 Braunschweig, Germany. [4]Max-Planck-Institut für Sonnensystemforschung, Justus-von-Liebig-Weg 3, 37077 Göttingen, Germany. [5]Deutsches Zentrum für Luft- und Raumfahrt, Institut für Planetenforschung, Rutherfordstraße 2, 12489 Berlin, Germany.

Received: 11 June 2021 Accepted: 20 October 2021
Published online: 09 November 2021

References

Alexeev II, Belenkaya ES, Bobrovnikov SYu, Slavin JA, Sarantos M (2008) Paraboloid model of Mercury's magnetosphere. J Geophys Res 113:A12210. https://doi.org/10.1029/2008JA013368

Anderson BJ, Johnson CL, Korth H, Winslow RM, Borovsky JE, Purucker ME et al (2012) Low-degree structure in Mercury's planetary magnetic field. J Geophys Res 117:E00L12. https://doi.org/10.1029/2012JE004159

Anderson BJ, Johnson CL, Korth H, Slavin JA, Winslow RM, Phillips RJ, McNutt RL Jr, Solomon SC (2014) Steady-state field-aligned currents at Mercury. Geophys Res Lett 41:7444–7452. https://doi.org/10.1002/2014GL061677

Andreeva VA, Tsyganenko NA (2016) Reconstructing the magnetosphere from data using radial basis functions. J Geophys Res 121:2249–2263. https://doi.org/10.1002/2015JA022242

Backus G (1986) Poloidal and toroidal fields in geomagnetic field modeling. Rev Geophys 24:75–109. https://doi.org/10.1029/RG024i001p00075

Backus G, Parker R, Constable C (1996) Foundations of geomagnetism. Cambridge University Press, Cambridge

Baumjohann W, Blanc M, Fedorov A, Glassmeier K-H (2010) Current systems in planetary magnetospheres and ionospheres. Space Sci Rev 152:99–134. https://doi.org/10.1007/s11214-010-9629-z

Bayer M, Freeden W, Maier T (2001) A vector wavelet approach to iono- and magnetospheric geomagnetic satellite data. J Atmos Solar-Terrestr Phys 63:581–597. https://doi.org/10.1016/S1364-6826(00)00234-0

Benkhoff J, van Casteren J, Hayakawa H, Fujimoto M, Laakso H, Novara M, Ferri P, Middleton HR, Ziethe R (2010) BepiColombo-Comprehensive exploration of Mercury: Mission overview and science goals. Planet Space Sci 85(1–2):2–20. https://doi.org/10.1016/j.pss.2009.09.020

Capon J (1969) High resolution frequency-wavenumber spectrum analysis. Proc IEEE 57:1408–1418. https://doi.org/10.1109/PROC.1969.7278

Cheng CZ, Zaharia S (2003) Field line resonances in quiet and disturbed time three-dimensional magnetospheres. J Geophys Res 108:1–18. https://doi.org/10.1029/2002JA009471

Engels U, Olsen N (1999) Computation of magnetic fields within source regions of ionospheric and magnetospheric currents. J Atmos Solar-Terrestr Phys 60:1585–1592. https://doi.org/10.1016/S1364-6826(98)00094-7

Exner W, Heyner D, Liuzzo L, Motschmann U, Shiota D, Kusano K, Shibayama T (2018) Coronal mass ejection hits mercury: A.I.K.E.F. hybrid-code results compared to MESSENGER data. Planet Space Sci 153:89–99. https://doi.org/10.1016/j.pss.2017.12.016

Exner W, Simon S, Heyner D, Motschmann U (2020) Influence of Mercury's exosphere on the structure of the magnetosphere. J Geophys Res 125:e27691. https://doi.org/10.1029/2019JA027691

Gauss CF (1839) Allgemeine Theorie des Erdmagnetismus: Resultate aus den Beobachtungen des magnetischen Vereins im Jahre 1838, edited by: Gauss, C. F. and Weber, W., 1-57, Weidmannsche Buchhandlung, Leipzig, 1839

Ganushkina NY, Liemohn MW, Dubyagin S, Daglis IA, Dandouras I, De Zeeuw DL, Ebihara Y, Ilie R, Katus R, Kubyshkina M, Milan SE, Ohtani S, Ostgaard

N, Reistad JP, Tenfjord P, Toffoletto F, Zaharia S, Amariutei O (2015) Defining and resolving current systems in geospace. Ann Geophys 33:1369–1402. https://doi.org/10.5194/angeo-33-1369-2015
Ganushkina NY, Liemohn MW, Dubyagin S (2018) Current systems in the Earth's magnetosphere. Rev Geophys. https://doi.org/10.1002/2017RG000590
Glassmeier K-H (2000) Currents in Mercury's magnetosphere, Magnetospheric Current Systems, Geophysical Monograph Series. American Geophysical Union, Washington. 118:371–380. https://doi.org/10.1029/GM118p0371
Glassmeier K-H, Auster H-U, Heyner D, Okrafka K, Carr C, Berghofer G, Anderson BJ et al (2010) The fluxgate magnetometer of the BepiColombo Mercury Planetary Orbiter. Planet Space Sci 58:287–299. https://doi.org/10.1016/j.pss.2008.06.018
Glassmeier K-H, Tsurutani BT (2014) Carl Friedrich Gauss - General Theory of Terrestrial Magnetism - a revised translation of the German text. Hist Geo Space Sci 5:11–62. https://doi.org/10.5194/hgss-5-11-2014
Grygorov K, Šafránková J, Němeček Z, Pi G, Přech L, Urbář J (2017) Shape of the equatorial magnetopause affected by the radial interplanetary magnetic field. Planet Space Sci 148:28–34. https://doi.org/10.1016/j.pss.2017.09.011
He M, Vogt J, Heyner D, Zhong J (2017) Solar wind controls on Mercury's magnetospheric cusp. J Geophys Res 122:6. https://doi.org/10.1002/2016JA023687
Heyner D, Auster H-U, Fornacon K-H, Carr C, Richter I, Mieth JZD, Kolhey P et al (2021) The BepiColombo planetary magnetometer MPO-MAG: What can we learn from the Hermean magnetic field? Space Sci Rev 217:52. https://doi.org/10.1007/s11214-021-00822-x
Iijima T, Potemra TA (1976) The amplitude distribution of field-aligned currents at northern high latitudes observed by Triad. J Geophys Res 81:2165–2174. https://doi.org/10.1029/JA081i013p02165
Jia X, Slavin JA, Gombosi TI, Daldorff LKS, Toth G, Holst B (2015) Global MHD simulations of Mercury's magnetosphere with coupled planetary interior: induction effect of the planetary conducting core on the global interaction. J Geophys Res Space Phys 120:4763–4775. https://doi.org/10.1002/2015JA021143
James MK, Imber SM, Bunce EJ, Yeoman TK, Lockwood M, Owens MJ, Slavin JA (2017) Interplanetary magnetic field properties and variability near Mercury's orbit. J Geophys Res. https://doi.org/10.1002/2017JA024435
James MK, Imber SM, Yeoman TK, Bunce EJ (2019) Field line resonance in the Hermean magnetosphere: structure and implications for plasma distribution. J Geophys Res 124:211–228. https://doi.org/10.1029/2018JA025920
Janhunen P, Kallio E (2004) Surface conductivity of Mercury provides current closure and may affect magnetospheric symmetry. Ann Geophys 22:1829–1837. https://doi.org/10.5194/angeo-22-1829-2004
Korth H, Anderson BJ, Acuña MH, Slavin JA, Tsyganenko NA, Solomon SC, McNutt RL (2004) Determination of the properties of Mercury's magnetic field by the MESSENGER mission. Planet Space Sci 52:733–746. https://doi.org/10.1016/j.pss.2003.12.008
Korth H, Anderson BJ, Gershman DJ, Raines JM, Slavin JA, Zurbuchen TH, Solomon SC, McNutt RL Jr (2014) Plasma distribution in Mercury's magnetosphere derived from MESSENGER Magnetometer and Fast Imaging Plasma Spectrometer observations. J Geophys Res 119:2917–2932. https://doi.org/10.1002/2013JA019567
Korth H, Tsyganenko NA, Johnson CL, Philpott LC, Anderson BJ, Al Asad MM, Solomon SC, McNutt RL Jr (2015) Modular model for Mercury's magnetospheric magnetic field confined within the average observed magnetopause. J Geophys Res 120:4503–4518. https://doi.org/10.1002/2015JA021022
Korth H, Johnson CL, Philpott LC, Tsyganenko NA, Anderson BJ (2017) A dynamic model of Mercury's magnetospheric magnetic field. Geophys Res Lett 44:10147–10154. https://doi.org/10.1002/2017GL074699
Leontyev SV, Lyatsky WB (1974) Electric fields and currents connected with y-component of interplanetary magnetic field. Planet Space Sci 22:811–819. https://doi.org/10.1016/0032-0633(74)90151-2
Liou K, Mitchell E (2019) Effects of the interplanetary magnetic field y component on the dayside aurora. Geosci Lett 6:11. https://doi.org/10.1186/s40562-019-0141-3
Mayer C, Maier T (2006) Separating inner and outer Earth's magnetic field from CHAMP satellite measurements by means of vector scaling functions and wavelets. Geophys J Int 167(3):1188–1203. https://doi.org/10.1111/j.1365-246X.2006.03199.x
Milan SE, Clausen LBN, Coxon JC, Carter JA, Walach M-T, Laundal K, Østgaard N, Tenfjord P, Reistad J, Snekvik K, Korth H, Anderson BJ (2017) Overview of solar wind-magnetosphere-ionosphere-atmosphere coupling and the generation of magnetospheric currents. Space Sci Rev 206:547–573. https://doi.org/10.1007/s11214-017-0333-0
Motschmann U, Woodward TI, Glassmeier K-H, Southwood DJ, Pinçon J-L (1996) Wavelength and direction filtering by magnetic measurements at satellite arrays: Generalized minimum variance analysis. J Geophys Res 101:4961–4966. https://doi.org/10.1029/95JA03471
Müller J, Simon S, Motschmann U, Schüle J, Glassmeier K-H, Pringle GJ (2011) A.I.K.E.F.: Adaptive hybrid model for space plasma simulations. Comp Phys Comm 182:946–966. https://doi.org/10.1016/j.cpc.2010.12.033
Olsen N (1997) Ionospheric F currents at middle and low latitudes estimated from Magsat data. J Geophys Res 102:4569–4576. https://doi.org/10.1029/96JA02949
Raines JM, Gershman DJ, Slavin JA, Zurbuchen TH, Korth H, Anderson BJ, Solomon SC (2014) Structure and dynamics of Mercury's magnetospheric cusp: MESSENGER measurements of protons and planetary ions. J Geophys Res 119:6587–6602. https://doi.org/10.1002/2014JA020120
Raines JM, DiBraccio GA, Cassidy TA, Delcourt DC, Fujimoto M, Jia X, Mangano V, Milillo A, Sarantos M, Slavin JA, Wurz P (2015) Plasma sources in planetary magnetospheres: Mercury. Space Sci Rev 192(1):91–144. https://doi.org/10.1007/s11214-015-0193-4
Romashets E, Vandas M (2020) Euler potentials for the Earth magnetic field with field-aligned currents. J Geophys Res 125:8. https://doi.org/10.1029/2020JA028153
Slavin JA, Imber SM, Raines JM (2021) A Dungey cycle in the life of Mercury's magnetosphere. Geophys Monogr Ser. https://doi.org/10.1002/9781119815624.ch34
Stern D (1967) Geomagnetic Euler potentials. J Geophys Res 72:3995–4005. https://doi.org/10.1029/JZ072i015p03995
Stern D (1970) Euler potentials. Am J Phys 38:494. https://doi.org/10.1119/1.1976373
Thébault E, Finlay CC, Beggan CD, Alken P, Aubert J, Barrois O et al (2015) International Geomagnetic Reference Field: the 12th generation. Earth Planets Space 67:79. https://doi.org/10.1186/s40623-015-0228-9
Toepfer S, Narita Y, Heyner D, Motschmann U (2020a) The Capon method for Mercury's magnetic field analysis. Front Phys 8:249. https://doi.org/10.3389/fphy.2020.00249
Toepfer S, Narita Y, Heyner D, Kolhey P, Motschmann U (2020b) Mathematical foundation of Capon's method for planetary magnetic field analysis. Geosci Instrum Method Data Syst 9:471–481. https://doi.org/10.5194/gi-9-471-2020
Toepfer S, Narita Y, Glassmeier K-H, Heyner D, Kolhey P, Motschmann U, Langlais B (2021a) The Mie representation for Mercury's magnetic field. Earth Planets Space 73:65. https://doi.org/10.1186/s40623-021-01386-4
Toepfer S, Narita Y, Heyner D, Motschmann U (2021b) Error propagation of Capon's minimum variance estimator. Front Phys 9:684410. https://doi.org/10.3389/fphy.2021.684410
Tsyganenko NA, Andreeva VA, Sitnov MI (2021) Reconstruction of magnetospheric storm-time dynamics using cylindrical basis functions and multi-mission data mining. J Geophys Res. 126:e2020JA028390. https://doi.org/10.1029/2020JA028390
Trondsen TS, Lyatsky W, Cogger LL, Murphree JS (1999) Interplanetary magnetic field By control of dayside auroras. J Atmos Sol-Terr Phys 61(11):829–840. https://doi.org/10.1016/S1364-6826(99)00029-2
Wardinski I, Langlais B, Thébault E (2019) Correlated Time-Varying Magnetic Field and the Core Size of Mercury. J Geophys Res 124:2178–2197. https://doi.org/10.1029/2018JE005835
Winslow RM, Anderson BJ, Johnson CL, Slavin JA, Korth H, Purucker ME, Baker DN, Solomon SC (2013) Mercury's magnetopause and bow shock from MESSENGER magnetometer observations. J Geophys Res 118(5):2213–2227. https://doi.org/10.1002/jgra.50237

Publisher's Note